AGU
ADVANCING EARTH AND SPACE SCIENCE

Geophysical Research Letters®

RESEARCH LETTER

Key Points:

- Lunar pits stay warmer than the surface during the night, with the floor maintaining temperatures >230 K according to computational models
- Caves stemming from lunar pits would behave like blackbody cavities at ~290 K and have nearly invariable temperatures far from the opening
- Lunar caves would provide a temperate, stable, and safe thermal environment for long term exploration and habitation of the Moon

Thermal and Illumination Environments of Lunar Pits and Caves: Models and Observations From the Diviner Lunar Radiometer Experiment

Tyler Horvath[1] [ORCID], **Paul O. Hayne[2], and David A. Paige[1]**

[1]Department of Earth, Planetary, and Space Sciences, University of California, Los Angeles, CA, USA, [2]Department of Astrophysical and Planetary Sciences, University of Colorado, Boulder, CO, USA

Abstract Lunar collapse pits may provide access to subsurface lava tubes of unknown extent. We present Diviner Lunar Radiometer measurements showing that the Mare Tranquillitatis and Mare Ingenii pits exhibit elevated thermal emission during the night, ~100 K warmer than the surrounding surface. Using these data, along with computational thermophysical models, we characterize the thermal environment inside pits and potential caves. Near the equator, peak day-time temperatures on regolith-covered pit floors can potentially reach >420 K, whereas temperatures beyond the opening in permanent shadow would maintain a nearly constant temperature of ~290 K, similar to that of a blackbody cavity in radiative equilibrium. Thermal IR measurements such as those of Diviner can readily detect pit thermal signatures but would be insensitive to the existence of caves they may host, as the latter would only induce a 0.1 K increase to night-time temperatures of the overlying surface.

Plain Language Summary Since the discovery of pits on the Moon by JAXA's SELENE spacecraft in 2009, there has been interest in whether they provide access to caves that could be explored by rovers and astronauts. These features are likely created by the ceiling of a lava tube (or more generally, cave) collapsing. Using data from the Diviner instrument aboard the Lunar Reconnaissance Orbiter, which has been continuously measuring the temperature of the lunar surface for over 11 years, we thoroughly characterized the environment of one prominent pit. Located in Mare Tranquillitatis, the pit's thermal environment is more hospitable compared to anywhere else on the Moon, with temperatures varying minimally around a comfortable 17°C (or 63° F) wherever the Sun does not shine directly. If a cave extends from a pit such as this, it too would maintain this comfortable temperature throughout its length, varying by less than 1°C over an entire lunar day. Although we cannot be completely certain of a cave's existence through remote observations, such features would open the door for future exploration and habitation on the Moon: they could provide shelter from dramatic temperature variations present elsewhere on the lunar surface.

1. Introduction

Pit craters are formed from the collapsed ceilings of subsurface void spaces, such as natural caves or lava tubes. Lava tube and cave are used interchangeably throughout the text. Collapse pits have been found on every major rocky body of the inner solar system (Davey et al., 2013; Haruyama et al., 2009; Kerber et al., 2011; Okubo & Martel, 1998; Wyrick et al., 2004). However, distinct overhangs have only been observed on Earth and the Moon. They are typically the result of a structural instability triggered by seismic activity, tectonism, and/or impacts (Okubo & Martel, 1998; Martellato et al., 2013). There are 16 confirmed collapse pit features on the Moon potentially stemming from lava tube networks (Wagner & Robinson, 2014) and many more resulting from the collapse of impact melt material. The former have diameters ranging from 15 to 150 m, spanning latitudes from −36° to 45°, most of which exist in the maria. Several pit craters on the Moon have verified overhangs (Wagner & Robinson, 2014), which naturally suggests they could be openings to lava tube networks.

While lava tubes may be responsible for many of the observed lunar collapse pits, evidence for intact caves is limited. Previous research using gravitational data from the Gravity Recovery and Interior Laboratory (GRAIL) spacecraft and radar data from the Lunar Radar Sounder (LRS) aboard the SELENE spacecraft has shown that the pit located in Marius Hills could be part of a lava tube system that extends for tens of kilometers (Chappaz et al., 2017; Kaku et al., 2017). The GRAIL data indicated a mass deficit along the rille that hosts the pit, and follow-up observations using LRS detected a transition between solid material and an empty cavity.

Supervision: Paul O. Hayne, David A. Paige
Validation: Tyler Horvath
Visualization: Tyler Horvath
Writing – original draft: Tyler Horvath, Paul O. Hayne, David A. Paige
Writing – review & editing: Paul O. Hayne, David A. Paige

Lunar pits and their potential caves have garnered much interest due to their exposures of sequences of lunar lava flows, as well as their potential to serve as operating bases for future exploration activities (e.g., Horz, 1985). Layered exposures within the pit walls indicate an accessible stratigraphy which could be exploited by a lander or rover to better understand lunar mare volcanism. Perhaps, punctuating discrete lava flows are intervals of regolith formation such that age-dating adjacent layers could provide estimates for the past meteoritic influx and rates of regolith formation (Kerber et al., 2019). Future human exploration activities may also take advantage of the protection offered by lunar pits and caves. Inside these cavities exposure to cosmic rays, solar radiation, micrometeorites, and harsh temperature extremes would be substantially reduced. Their location on the Moon's nearside also has the potential advantage of direct-to-Earth communications.

We investigated the thermal signatures of collapse pits with the Diviner Lunar Radiometer Experiment aboard the Lunar Reconnaissance Orbiter (LRO). While others have speculated regarding the benign thermal environments of pits and caves, confirmation has been lacking. Here, we present the Diviner measurements and models used to constrain the temperatures and illumination conditions inside the pits and their potential caves.

2. Approach and Methods

2.1. Diviner Data

Diviner is a nine-channel radiometer with solar and infrared spectral bands. Channels 1–2 measure broadband solar reflectance, channels 3–5 are positioned for mid-IR mineralogy, and channels 6–9 measure thermal-IR emission from ~12.5 to 400 μm wavelength (Paige, Foote, et al., 2010). Diviner is capable of measuring surface brightness temperatures to within ±3 K from 50 to 75 K and ±1 K accuracy at >75 K, allowing for accurate temperature readings at all local times and all locations except the coldest of permanently shadowed regions (Paige, Siegler, et al., 2010). The instrument operates in a push-broom imaging mode, capturing 189 unique spatial and spectral measurements every 0.128 s, resulting in a nominal spatial resolution of ~128 pixels per degree (ppd) (~250 m resolution at the equator). Diviner's multi-spectral measurements also enable measurement of sub-pixel temperature variations, which are recorded as "anisothermality" in the brightness temperature spectrum (Bandfield et al., 2011).

Diviner's instantaneous field of view (IFOV) is 3.4×6.7 mrad, equivalent to 160×320 m from an orbital altitude of 50 km (Paige, Foote, et al., 2010). Even the largest pits (e.g., Tranquillitatis, ~100 m in diameter) are therefore unresolved, though they can occupy an appreciable fraction of the IFOV at lower spacecraft altitudes. Furthermore, spacecraft motion and Diviner's ~128 ms integration time smears the signal primarily in the along-track (N–S) direction. Therefore, our radiometric model includes the sub-pixel temperature distribution, as well as the effects of in-track smearing due to spacecraft motion (cf. Hayne et al., 2010). As described in the Supporting Information, we modeled the 2-D angular response function of Diviner's detectors to find the sub-pixel pit temperatures that best recreate the smeared temperature profile.

For this investigation, we used topography corrected Level 1b data focusing primarily on channels 6, 7, and 8, operating from 12.5 to 25 μm, 25–50 μm, and 50–100 μm, respectively (Paige, Schofield, et al., 2010). Using localized data from July 2009 to March 2019, we retrieved all night-time measurements from 8 p.m. to 4 a.m. Local Solar Time (LST), allowing us to isolate the heightened pit temperature from the individual Diviner measurements. Additionally, we concentrated on emission angles <10° to better constrain the pit floor temperatures, rather than the floor and walls together, which would add unneeded complexity and increased uncertainty. From these data and known geometries for the Tranquillitatis pit, we were able to construct a night-time temperature curve, which we then compare directly to thermal models.

2.2. Thermal Modeling

2.2.1. The 2-D and 3-D Models

In addition to analyzing the thermal data from Diviner, we created and ran time-dependent 2-D and 3-D thermal models using COMSOL Multiphysics® to interpret the observations of the Tranquillitatis pit. These models are necessary to understand the complex geometry and heat transfer that could lead to the elevated thermal signatures indicated by the Diviner measurements. We used the 2-D models to simulate steady-state equilibrium conditions of pits with and without caves, while the 3-D models provided the dynamic thermal variations of the pit. The 2-D

models were run for 500 Earth years to reach equilibrium, while the more computationally expensive 3-D models were run for only two lunar days. Overviews of these models are provided here, while a more detailed description is given in the supplementary information.

We explored the possibility of implementing a 2-D axisymmetric model but found that a spatially infinite 2-D model more accurately captures the physical intricacies of the pit-cave system. Due to the highly thermally insulative lunar regolith, the conductive heat losses become negligible such that both modeling methods produce physically realistic blackbodies, but scale differently when cave length is increased. Because these caves likely have a width on the same order as the pit diameter, a ratio which is well-preserved in an infinite model but not maintained in an axisymmetric model for longer caves, the spatially infinite 2-D model will more closely approximate the 3-D geometry of a potential cave. Additionally, spatially infinite models can simulate solar motion, which is required to properly account for the distribution of radiative energy within the pit-cave system. Together these properties allow us to acquire a realistic cave equilibrium temperature and provide a basis for comparing the model results to the Diviner data.

For each model, we used the standard thermophysical properties of lunar regolith (Hayne et al., 2017) and lunar basaltic rock (Bandfield et al., 2011) to determine what geometry and materials best match the Diviner data. For some thermophysical properties, there are known temperature and/or depth dependencies (Hayne et al., 2017; Vasavada et al., 2012); however, we neglect depth dependence as the vertical scale of the models extend well beyond the density scale height of the material and its diurnal thermal skin depth, and it would cause the models to become unnecessarily complex. In all models we include an interior heat flux of 18 mW/m^2 (Hayne et al., 2017), lateral boundary conditions of zero thermal heat flux, and appropriate solar motion. In the 3-D models, we used NASA Jet Propulsion Laboratory's (JPL) HORIZONS ephemeris generator (Giorgini, 2015) to obtain the Sun's location relative to the Mare Tranquillitatis pit. In the 2-D model, we simply set the Sun to move circularly perpendicular to the plane of the model surface at 1 AU, which is an accurate approximation given the Tranquillitatis pit's nearly equatorial location and the Moon's low obliquity relative to the Sun.

To implement pit and cave geometry in the 3-D models, we used complex meshes created at JPL using stereographic pairs of the Tranquillitatis pit from LRO's Narrow Angle Camera (NAC) with manual extrapolation underneath the pit's overhang (Kerber et al., 2019). This method produces a rough; though representative, model of the pit's geometry containing ∼4500 polygons at ∼5 m scale. For the 2-D models, we used established geometries as a template, and then extrapolated the subsurface model geometry. The pit diameter, depth, and height of the overhang for the pit as derived from the LRO NAC images are approximately 100, 100, and 40 m, respectively (Wagner & Robinson, 2014). Collapse material on the pit floor was included to better simulate expected geometries and to allow for the testing of different floor materials. The initial model temperatures were 260 K throughout, which is the approximate annual average surface temperature at the Tranquillitatis pit (Hayne et al., 2017; Williams et al., 2017), but we also ran models with temperatures initialized to 300 K to ensure the models converged.

2.2.2. The 1-D Models

An intriguing possibility is that a warm cave interior may be detectable by Diviner if enough heat is conducted to the surface above. To place constraints on the required subsurface temperatures and heat fluxes that would result in a detectable surface temperature change, we used a 1-D thermal model using COMSOL®. In one version of this model, we set the lower boundary condition using the equilibrium temperatures from the 2-D model described in Section 2.2.1, and in another version, we used the interior heat flow as was done in the 2-D and 3-D models. The former would be the best-case scenario for Diviner to measure an increase in surface temperature. Both used standard regolith thermophysical properties with depth dependence (Hayne et al., 2017). The domain used is 5-m long composed of sub-millimeter mesh elements near the surface, with exponentially increasing spacing between mesh elements as depth increases. This model exhibits an ideal case for a warm subsurface feature to affect observed surface temperatures.
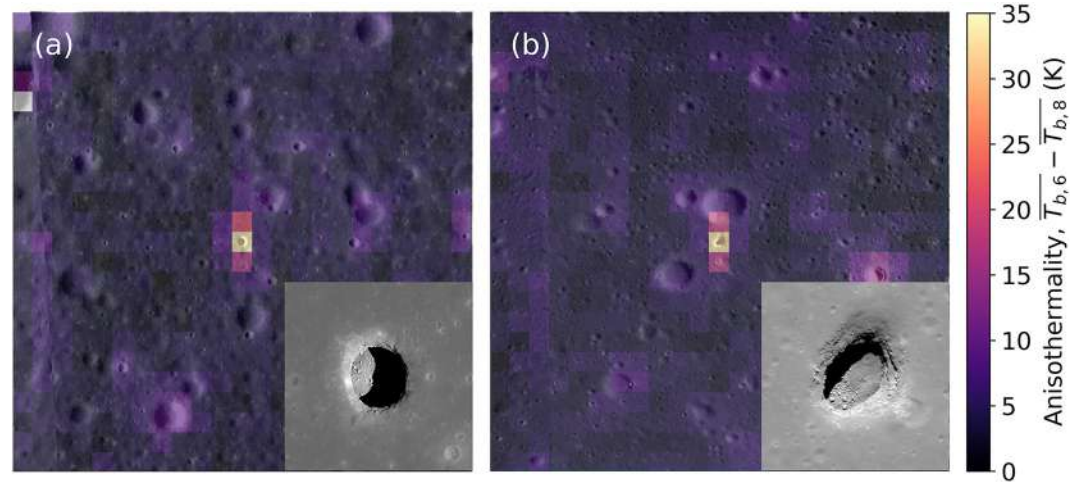
Figure 1. 250 m per pixel mapping using the mean of all Channels 6 and 8 brightness temperature measurements taken between 9 p.m. and 4 a.m. LST for (a) the Mare Tranquillitatis pit and (b) the Mare Ingenii pit. This data presented are anisothermality, that is, the variability of temperatures within a single bin, given by $T_{b,6} - T_{b,8}$. The color bar, x, and y dimensions are all scaled equally and are overlaid by LROC NAC mosaics of the region for context. Inset images are from LRO NAC M126710873R for the Tranquillitatis pit and NAC M171835900L for the Ingenii pit and represent the view within the warm central pixel of the anisothermality map.

3. Results

3.1. Diviner Data Analysis

The Diviner data indicate strong anisothermality centered on the Mare Tranquillitatis pit (33.221°E 8.334°N) (Figure 1a) caused by a mix of warm and cold surfaces within the pixel (Figures S5 and S7 in Supporting Information S1). Similarly, another heightened signal is apparent at the Mare Ingenii pit (166.055°E 35.950°S) (Figure 1b). Although Diviner measures a difference of only ∼30 K between the channels, the true difference between the pit's temperature, and the background is much higher as the pit's size is only a fraction of a detector's IFOV. For example, given the pits' diameters to be ∼100 m, the pits constitute a maximum of ∼20% of a detector's IFOV at the lowest spacecraft altitudes where data are available (∼40 km).

We derived pit floor temperatures from each unique night-time observation of the Tranquillitatis pit between 8 p.m. and 4 a.m. LST and constructed a night-time temperature profile. By using Diviner's 2-D angular response function, spectral response function, and measured background temperatures, we can use a chi-square goodness-of-fit test (Supporting Information) to derive the sub-pixel pit temperature that best reproduces the Diviner Measurements. With this analysis, we see temperatures with one-sigma confidence in excess of 200 K over the entire time range of 8 p.m. to 4 a.m. LST, though most of the best fit data are centered between 250 and 290 K (Figure 3). Bandfield et al. (2011) showed that even a pure rock slab with very high thermal inertia (∼1570 J m^{-2} K^{-1} s$^{-½}$) will cool to 185 K by the end of the lunar night. Therefore, another mechanism must be invoked to produce the elevated temperatures. We used computational thermal models to understand what geometries and materials could best reproduce the measured temperatures. From this analysis, we can compare the night-time temperature profile curve to the results of the 2-D thermal models.

3.2. Thermal Model Results

3.2.1. The 2-D Model Results

The 2-D model represents a physically realistic scenario without the computational cost of a 3-D model. We ran several cases (Figure 2a): extended cave with rock-like collapse material (Figure 2b); extended cave with regolith-like collapse material (Figure 2c); shallow cave with rock-like collapse material; and (Figure 2d) shallow cave with regolith-like collapse material, each model used rock-like properties throughout the bulk and was overlaid by 5 m of regolith. These test cases were intended to determine whether the presence of an extended cave could be inferred from pit floor temperatures.
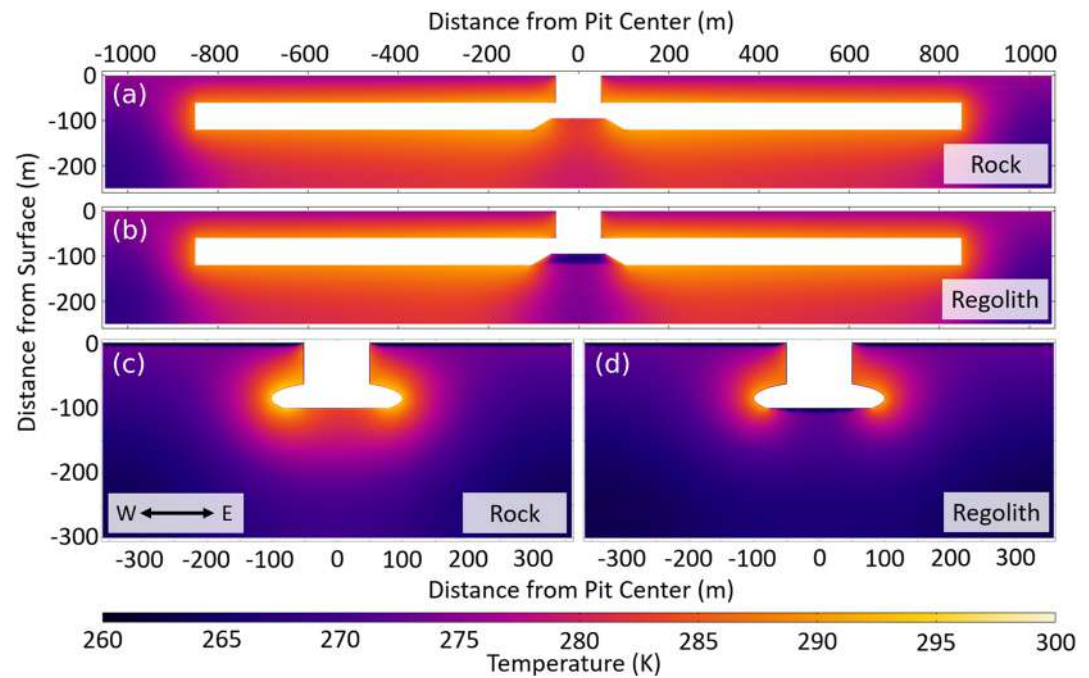
Figure 2. 2-D model equilibrated midnight temperatures with different geometries and pit floor materials. Indicated within each frame is the floor composition, while the bulk material remains rock throughout. Subfigures 2(a) and 2(b) are described as having an extended cave, while 2(c) and 2(d) have a shallow cave.

Results of the 2-D models (Figure 2) show that all combinations of geometry and pit floor composition stay above 230 K at equilibrium, even late in the night when the surrounding surface is ∼100 K. We find that there is little temperature difference between pits with shallow or extended caves, and only a small difference of 25 K between a pit whose floor is composed of pure rock or pure regolith (Figure 3). The models also show that a regolith covered floor could reach temperatures greater than 420 K at noon (Figures S3 and S4 in Supporting Information S1), ∼20 K higher than the warmest equatorial surfaces measured by Diviner (Williams et al., 2017). Moreover, the equilibrium temperature of a cave is ∼290 K with minimal temperature variations wherever the sun cannot illuminate directly (Figures S3 and S4 in Supporting Information S1).

Analytically, the equilibrium temperature (T_{eq}) of a blackbody cavity is determined from a balance between the mean diurnal insolation and infrared emission and is given by,

$$T_{eq} = \left(\frac{F\cos\varphi}{\pi\sigma} \right)^{1/4}, \tag{1}$$

where F is the solar constant (∼1361 W/m^2), φ is the latitude, and σ is the Stefan-Boltzmann constant. An ideal blackbody cavity situated at the equator would result in an equilibrium temperature of ∼296 K. This is nearly equivalent to temperatures seen in the 2-D model within the unilluminated regions of the subsurface void. This equilibrium temperature is shown in Figure 3 and is treated as a physically realistic upper bound for the Diviner measurement of pit temperatures, whereas the error is determined by the Chi-square model fitting.

3.2.2. The 1-D Model Results

From the 1-D models, we determined that the elevated temperatures caused by the presence of a cave would produce a perturbation at the surface of only ∼0.1 K (Figure S1 in Supporting Information S1). Within the top 20 cm, the temperature perturbation is <2 K. This result is due to the highly insulating properties of the overlying regolith layer, thereby allowing a strong thermal gradient in the upper few meters. In effect, the cave can maintain almost any temperature without being able to lose its heat effectively through conduction to the surface, rendering the subsurface cave effectively invisible to an orbit-based thermal detector, such as Diviner. Below the thermal
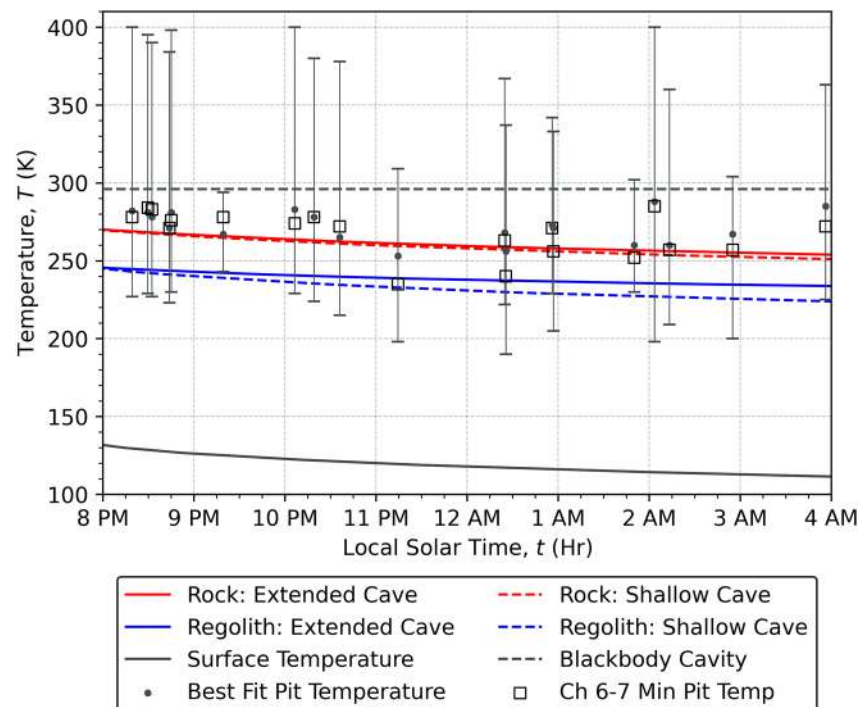
Figure 3. 2-D thermal models (lines) compared to Tranquillitatis pit temperatures derived from night-time Diviner Data using 19 separate orbits (points). Circular points with 1σ error were determined through Chi-square model fitting while the square points are the minimum pit temperature needed to reach the maximum measured temperatures in Diviner channels 6 and 7.

skin depth, ∼10 cm deep (Hayne et al., 2017), the difference in thermal gradient becomes more apparent and temperatures increase more rapidly with depth.

3.2.3. The 3-D Model Results

The purpose of the 3-D models is to use realistic geometry to evaluate the variability of the pit's temperatures and illumination with respect to azimuth and depth within the pit. Due to computational costs, these models simulate only two lunar days and the subsurface elements do not fully equilibrate during this period. These models are also composed uniformly of regolith or rock, unlike the heterogeneous 2-D models. However, this still allows us to investigate the basic features that emerge when considering 3-D geometry. Figure 4 shows examples of surface temperature curves for different locations within the pit and on the surrounding surface.

Due to daily solar motion, all areas of the pit have very different illumination conditions throughout the day, which leads to a very dynamic thermal profile and each wall's peak temperature occurring at different times. While the Tranquillitatis pit is located at a near-equatorial latitude of 8.334° N, the models show that it nonetheless experiences an asymmetry in the thermal conditions between the North and South sides of the pit floor and wall. Again, the model predicts high maximum pit floor temperatures of ∼415 K with a regolith covered floor. This effect is not solely caused by direct heating of the pit floor by the Sun but also by the thermal radiation from the pit walls and underneath the overhang. Therefore, the Tranquillitatis pit specifically may be the hottest location on the Moon and is by far the warmest location during the lunar night. In contrast, when the floor is covered by rock, the day/night temperature contrast is damped, with peak day-time temperatures of ∼390 K and minimum night-time temperatures of ∼230 K.

4. Discussion

The model results show that the thermal environments inside pits and caves are moderated substantially more than the surface. Comparison of the 2-D model with an analytical energy balance model indicates that cave temperatures can be closely approximated as a blackbody; the cave's temperature would be nearly constant and
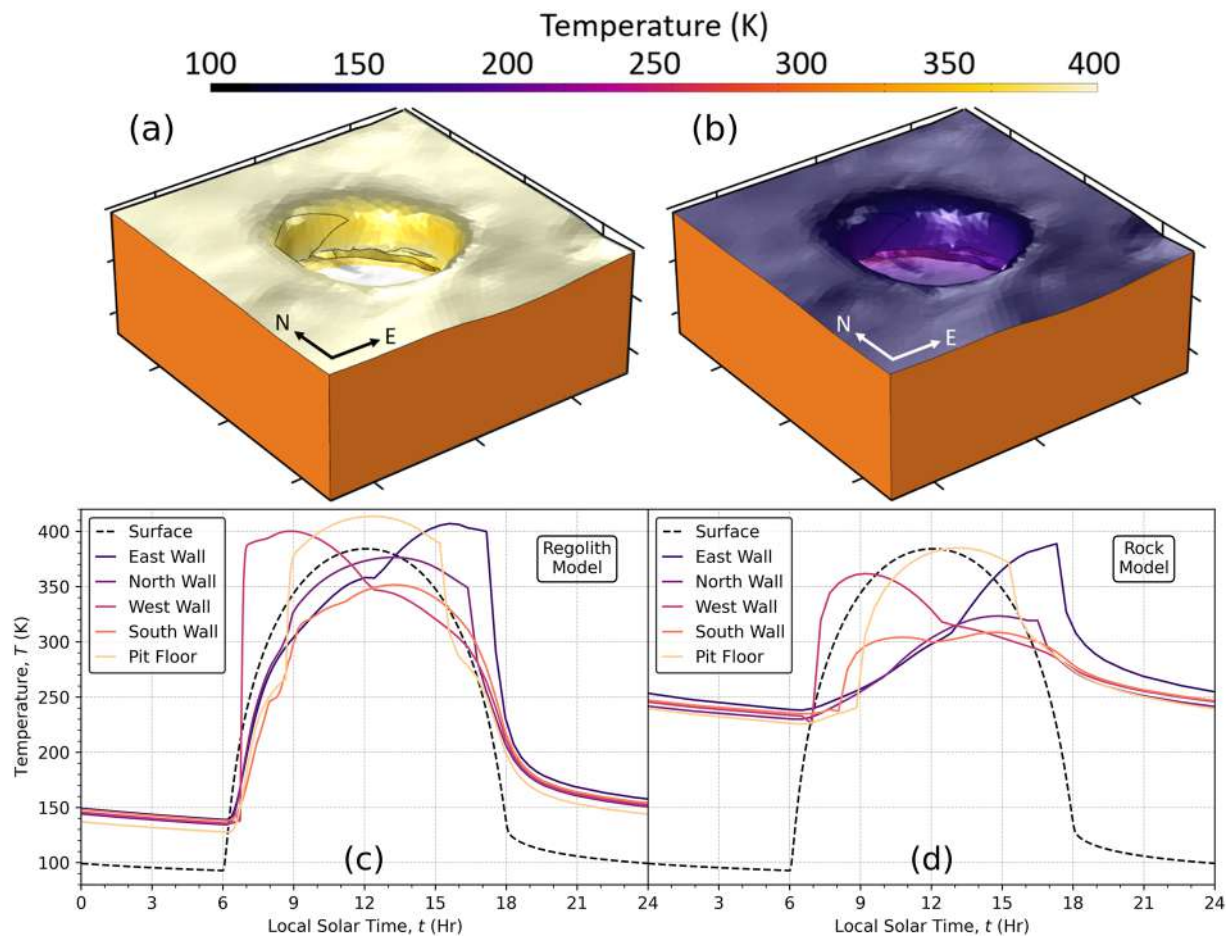
Figure 4. Uniform regolith 3-D model at (a) noon and (b) midnight, alongside diurnal curves at various locations along the pit walls 30 m below the surface for the (c) regolith and (d) rock models. The surface temperature reference curve is the result of the 1-D thermal model with the heat flow bottom boundary condition.

isothermal at ~290 K. This approximation holds if the surface area internal to the cave is large, compared to that of the pit through which radiation enters and exits. Geophysical sounding of the subsurface could provide valuable constraints on the thermal environment inside a cave, through detailed thermal models like those presented here. A microwave radiometer, such as the 3 GHz channel of the Chang'e MRM experiments could potentially observe the increase in temperature (Siegler & Feng, 2017); however, their observation footprint on the scale of tens of km would not resolve features the size of a potential subsurface cave near a pit. If such an instrument had higher spatial resolution, the presence of a cave could potentially be determined, and if it were used by astronauts or a rover in situ, the precise extent of the cave may be measurable.

Thermophysical properties (i.e., thermal inertia) are shown to have a significant impact on the diurnally varying temperatures of the pit walls and floor. However, the Diviner data are insufficient to directly constrain these properties due to the small size of the pits relative to the detector IFOV. To better constrain these thermophysical properties, we would require spatially resolved measurements (<100 m) of the pit floor and/or measurement errors of <10 K for the derived sub-pixel pit floor temperatures. Absent further data, our results are consistent with either a rocky or regolith-covered pit floor. Based on geological evidence (Wagner & Robinson, 2014) it was found that the pit walls are composed of rock, while the pit floor is a mixture of rock and regolith. Regardless of the thermophysical properties, temperatures under the overhang where the sky is not visible are nearly isothermal at ~290 K.

A rover or astronaut descending from the surface into a pit would experience rapidly changing illumination and temperature conditions (Figure 4). Furthermore, these conditions would depend on azimuthal location within the pit: where morning shadows are prominent on the eastern wall, and afternoon shadows are prominent on the western wall. In the northern hemisphere, the south wall would have the most benign thermal conditions with

temperatures reaching only 350 K at midday. Scattered sunlight is likely pronounced even within the shadows, potentially allowing optical imaging and spectroscopy measurements. As distance to the pit floor decreases, day-time temperatures increase substantially up to a maximum value of ∼415 K for a regolith-covered floor—potentially the warmest temperatures found anywhere on the Moon. Night-time pit floor temperatures are more benign, ∼100–130 K warmer than the surface above (Figure 4). Although the 3-D model reveals complex illumination and thermal conditions on the pit walls and floor, these variations are negligible inside a cave. Our results also indicate that a cave would not be detectable through its influence on surface temperatures due to the extremely insulating nature of lunar regolith.

5. Conclusions

The Mare Tranquillitatis and Mare Ingenii pits host some of the most unique thermal environments on the Moon. Their geometries make lunar pits effective heat traps, with peak temperatures up to ∼20 K warmer than the surrounding surface during the day. Night-time temperatures inside the pits are also warmer by ∼100 K. With agreement between computational models and temperature measurements from Diviner, we conclude that low-latitude pits maintain interior night-time surface temperatures of >200 K. These features also have the potential to host caves with a near constant, yet relatively clement 290 K temperature throughout the entire year. Furthermore, the Tranquillitatis pit is likely to host the highest day-time temperatures on the entire Lunar surface, over 415 K, owing to its unique near equatorial location and cylindrical geometry. For long term colonization and exploration of the Moon, pits may provide a desirable habitat: they are largely free from the constant threats of harmful radiation, impacts, and extreme temperatures. Thus, pits and caves may offer greater mission safety than other potential base station locales, providing a valuable stepping stone for sustaining human life beyond Earth.

Data Availability Statement

All associated Diviner data (Paige, Schofield, et al., 2010) and python code, including all of the python code's outputs, are available online through Zenodo at https://doi.org/10.5281/zenodo.6778129. COMSOL Multiphysics® version 5.6 and its Heat Transfer Module were used for this research and requires the purchase of a license to download at https://www.comsol.com.

References

Bandfield, J. L., Ghent, R. R., Vasavada, A. R., Paige, D. A., Lawrence, S. J., & Robinson, M. S. (2011). Lunar surface rock abundance and regolith fines temperatures derived from LRO Diviner Radiometer data. *Journal of Geophysical Research*, *116*(E12). https://doi.org/10.1029/2011JE003866

Chappaz, L., Sood, R., Melosh, H. J., Howell, K. C., Blair, D. M., Milbury, C., & Zuber, M. T. (2017). Evidence of large empty lava tubes on the Moon using GRAIL gravity. *Geophysical Research Letters*, *44*, 105–112. https://doi.org/10.1002/2016GL071588

Davey, S. C., Ernst, R. E., Samson, C., & Grosfils, E. B. (2013). Hierarchical clustering of pit crater chains on Venus. *Canadian Journal of Earth Sciences*, *50*(1), 109–126. https://doi.org/10.1139/cjes-2012-0054

Giorgini, J. D. (2015). Status of the JPL horizons ephemeris system. *IAU General Assembly*, *29*, 2256293.

Haruyama, J., Hioki, K., Shirao, M., Morata, T., Hiesinger, H., van der Bogert, C. H., et al. (2009). Possible lunar lava tube skylight observed by SELENE cameras. *Geophysical Research Letters*, *36*(21). https://doi.org/10.1029/2009gl040635

Hayne, P. O., Bandfield, J. L., Siegler, M. A., Vasavada, A. R., Ghent, R. R., Williams, J. P., et al. (2017). Global regolith thermophysical properties of the Moon from the diviner lunar radiometer experiment. *Journal of Geophysical Research: Planets*, *122*(12), 2371–2400. https://doi.org/10.1002/2017JE005387

Hayne, P. O., Greenhagen, B. T., Foote, M. C., Siegler, M. A., Vasavada, A. R., & Paige, D. A. (2010). Diviner lunar radiometer observation of the LCROSS impact. *Science*, *330*(6003), 477–479. https://doi.org/10.1126/science.1197135

Horz, F. (1985). Lava tubes: Potential shelters for habitats. In W. W. Mendell (Ed.), *Lunar bases and space activities of the 21st century* (p. 405). Lunar and Planetary Institute.

Kaku, T., Haruyama, J., Miyake, W., Kumamoto, A., Ishiyama, K., Nishibori, T., et al. (2017). Detection of intact lava tubes at Marius Hills on the Moon by SELENE (Kaguya) lunar radar sounder. *Geophysical Research Letters*, *44*(20), 10–155. https://doi.org/10.1002/2017gl074998

Kerber, L., Denevi, B. W., Nesnas, I., Keszthelyi, L., Head, J. W., Pieters, C., et al. (2019). Moon Diver: A discover mission concept for understanding secondary crust formation through the exploration of a lunar mare pit cross-section. *Paper Presented at 50th Annual Lunar and Planetary Science Conference*, Abstract No. 1163.

Kerber, L., Head, J. W., Blewett, D. T., Solomon, S. C., Wilson, L., Murchie, S. L., et al. (2011). The global distribution of pyroclastic deposits on Mercury: The view from MESSENGER flybys 1–3. *Planetary and Space Science*, *59*(15), 1895–1909. https://doi.org/10.1016/j.pss.2011.03.020

Martellato, E., Foing, B. H., & Benkhoff, J. (2013). Numerical modelling of impact crater formation associated with isolated lunar skylight candidates on lava tubes. *Planetary and Space Science*, *86*, 33–44. https://doi.org/10.1016/j.pss.2013.06.010

Okubo, C. H., & Martel, S. J. (1998). Pit crater formation on Kilauea volcano, Hawaii. *Journal of Volcanology and Geothermal Research*, *86*(1–4), 1–18. https://doi.org/10.1016/S0377-0273(98)00070-5

Paige, D. A., Foote, M. C., Greenhagen, B. T., Schofield, J. T., Calcutt, S., Vasavada, A. R., et al. (2010). The lunar reconnaissance orbiter diviner lunar radiometer experiment. *Space Science Reviews*, *150*(1–4), 125–160. https://doi.org/10.1007/s11214-009-9529-2

Paige, D. A., Schofield, J. T., Calcutt, S. B., Avis, C. C., Mortensen, H. B., & Sullivan, M. T. (2010). LRO-L-DLRE-4-RDR-V1.0, NASA Planetary Data System.

Paige, D. A., Siegler, M. A., Zhang, J. A., Hayne, P. O., Foote, E. J., Bennett, K. A., et al. (2010). Diviner lunar radiometer observations of cold traps in the Moon's south polar region. *Science*, *330*(6003), 479–482. https://doi.org/10.1126/science.1187726

Siegler, M. A., & Feng, J. (2017). Microwave remote sensing of lunar subsurface temperatures: Reconciling MRM and LRO diviner. *Paper presented at 47th Lunar and Planetary Science Conference*, Abstract No. 1705.

Vasavada, A. R., Bandfield, J. L., Greenhagen, B. T., Hayne, P. O., Siegler, M. A., Williams, J. P., & Paige, D. A. (2012). Lunar equatorial surface temperatures and regolith properties from the Diviner Lunar Radiometer Experiment. *Journal of Geophysical Research*, *117*(E12). https://doi.org/10.1029/2011JE003987

Wagner, R. V., & Robinson, M. S. (2014). Distribution, formation mechanisms, and significance of lunar pits. *Icarus*, *237*, 52–60. https://doi.org/10.1016/j.icarus.2014.04.002

Williams, J. P., Paige, D. A., Greenhagen, B. T., & Sefton-Nash, E. (2017). The global surface temperatures of the Moon as measured by the diviner lunar radiometer experiment. *Icarus*, *283*, 300–325. https://doi.org/10.1016/j.icarus.2016.08.012

Wyrick, D., Ferrill, D. A., Morris, A. P., Colton, S. L., & Sims, D. W. (2004). Distribution, morphology, and origins of Martian pit crater chains. *Journal of Geophysical Research*, *109*(E6). https://doi.org/10.1029/2004je002240

References From the Supporting Information

Foote, E. J., Paige, D. A., Shepard, M. K., Johnson, J. R., & Biggar, S. (2020). The bidirectional and directional hemispheric reflectance of Apollo 11 and 16 soils: Laboratory and Diviner measurements. *Icarus*, *336*, 113456. https://doi.org/10.1016/j.icarus.2019.113456

Howell, J. R., Mengüç, P. M., Daun, K., & Siegel, R. (2020). *Thermal radiation heat transfer* (7th ed.). CRC Press. https://doi.org/10.1201/9780429327308

Nesnas, I. A., Kerber, L., Parness, A., Kornfeld, R., Sellar, G., McGarey, P., et al. (2019). Moon Diver: A discovery mission concept for understanding the history of secondary crusts through the exploration of a lunar mare pit. *2019 IEEE Aerospace Conference* (pp. 1–23). IEEE. https://doi.org/10.1109/AERO.2019.8741788

Piqueux, S., & Christensen, P. R. (2009). A model of thermal conductivity for planetary soils: 1. Theory for unconsolidated soils. *Journal of Geophysical Research*, *114*(E09005). https://doi.org/10.1029/2008JE003308

Siegler, M. A., & Smrekar, S. E. (2014). Lunar heat flow: Regional prospective of the Apollo landing sites. *Journal of Geophysical Research: Planets*, *119*, 47–63. https://doi.org/10.1002/2013JE004453